Hindawi
Journal of Spectroscopy
Volume 2023, Article ID 1679035, 10 pages
https://doi.org/10.1155/2023/1679035

Research Article

Synthesis and Characterization of PANI/$ZnFe_2O_4$ nRs with Different Doping Concentrations for Potential Applications in Various Fields

Taymour A. Hamdalla,[1,2] **Meshari M. Aljohani**,[3] **and Abdulrhman M. Alsharari**[1]

[1]*Physics Department, Faculty of Science, University of Tabuk, Tabuk, Saudi Arabia*
[2]*Physics Department, Faculty of Science, Alexandria University, Alexandria, Egypt*
[3]*Chemistry Department, Faculty of Science, University of Tabuk, Tabuk, Saudi Arabia*

Correspondence should be addressed to Taymour A. Hamdalla; t-ahmed@ut.edu.sa

Received 12 September 2023; Revised 14 October 2023; Accepted 17 October 2023; Published 25 October 2023

Academic Editor: Pedro D. Vaz

The wide-ranging potential of polyaniline (PANI) composites in energy storage, electrochemical, sensing, and electromagnetic shielding applications emphasizes researchers to improve its properties. Here, the doping of $ZnFe_2O_4$ nRs by 1, 3, and 5 wt. % within polyaniline has been done. Then, we characterize the doped material using techniques such as scanning electron microscopy (SEM), X-ray diffraction (XRD), thermal gravimetric analysis (TGA), and Fourier-transform infrared spectroscopy (FTIR) to verify the successful incorporation of polyaniline onto the nRs. TGA showed that doping of PANI with $ZnFe_2O_4$ nRs enhanced the interfacial interactions between the two components. This provided a more stable matrix structure and enhanced the thermal stability of the composite. The transmission of light has been increased by about 18% due to the increase in crystallinity accompanied by $ZnFe_2O_4$ doping. As the $ZnFe_2O_4$ nRs doping rose, our PANI samples' optical band gap values slightly decreased by about 10%. In addition, it has been found that the optical characteristics such as refractive index, extension coefficient, surface, and volume energy loss function essentially showed $ZnFe_2O_4$ doping dependency. The nonlinear constants of the doped samples have increased due to the new charge carriers and altered the electronic and optical properties of the composite material. Our obtained results show that PANI@ $ZnFe_2O_4$ nRs have potential applications such as optical sensors, electrochemical, optoelectronics, and photocatalysis.

1. Introduction

Polyaniline (PANI) composites have shown great potential in various applications due to their unique properties such electrical conductivity, thermal stability, and mechanical properties [1]. It can conduct electricity in its doped (oxidized) state, making it useful for electronic and electrochemical applications [2]. PANI can be easily modified to achieve different optical and electrical characteristics [3]. By adjusting its doping level, conductivity can be controlled, making it adaptable for a wide range of applications. It can be synthesized through a relatively simple and cost-effective process. This makes it attractive for large-scale production and commercial applications. Polyaniline has shown promise in various fields, including electronics, energy storage (e.g., batteries and supercapacitors), sensors, corrosion protection, and actuators. PANI is a conductive polymer that exhibits favorable optical properties, such as high transparency and tunable absorption characteristics [4].

$ZnFe_2O_4$ nanoribbons ($ZnFe_2O_4$ nRs) are considered a fascinating material with unique structural properties and potential applications [5]. They are nanostructures composed of zinc, iron, and oxygen atoms arranged in a specific configuration. These nRs typically have a ribbon-like shape, with a length much greater than their width or height [6]. Their size, shape, and surface properties can influence their overall behavior and performance. The high aspect ratio of nRs can promote novel electronic, magnetic, and optical

properties that are not present in bulk materials [7]. As for potential applications, $ZnFe_2O_4$ nRs have been extensively studied in various fields. One notable application is in energy storage devices, like lithium-ion batteries. The unique structure of the nRs allows for improved electrode performance, such as enhanced lithium diffusion and increased capacity [8]. Additionally, $ZnFe_2O_4$ nRs have shown promise in catalysis [9]. Their large surface area and high reactivity make them suitable for applications such as water splitting, where they can act as efficient catalysts to produce hydrogen.

Furthermore, these nRs have been explored in the field of sensors due to their exceptional sensitivity to certain gases and chemicals [10]. They can be utilized in gas sensors, biosensors, and environmental monitoring devices. In terms of optical properties, the doping of $ZnFe_2O_4$ nRs with polyaniline can result in enhanced light absorption and emission properties [11]. This can be beneficial for applications such as optoelectronics, where efficient light absorption and emission are crucial. Composites of Fe_2O_4 nRs-based polymer for magnetic application have been done by Tong et al. [12]. This study explores the synthesis and characterization of $ZnFe_2O_4$ nanoribbon-based polymer composites for magnetic applications. Alshammari et al. enhanced electrical conductivity in PVC/PVP with $ZnFe_2O_4$ composites, and they achieved the improvement in the electrical conductivity by incorporating PVC/PVP with $ZnFe_2O_4$ in various polymer matrices [13]. They discussed the influence of nanoribbon concentration and orientation on the conductivity of the composites, highlighting their potential for applications in flexible electronics and conductive coatings. Optical properties of $ZnFe_2O_4$ nanoribbon-polymer composites for photonic applications have been investigated by Lee [14]. This research team examined the optical properties of $ZnFe_2O_4$ nanoribbon-polymer composites, emphasizing their potential for photonic applications. They investigated the tunable optical behavior of composites and discussed their potential in areas such as optical sensors, waveguides, and photovoltaics. These studies highlight the promising potential of $ZnFe_2O_4$ nRs doped in polymers for a wide range of applications, including magnetic devices, electrical conductivity enhancement, and optical functionalities.

The doping process itself plays a crucial role in achieving the desired optical and electrical properties [15, 16]. The concentration and distribution of polyaniline within the nRs, as well as the doping process conditions, can impact the final material's characteristics. Optimization of the doping process is necessary to achieve the desired properties and create nanocomposites that exhibit the best combination of optical and electrical performance [17]. Overall, doping $ZnFe_2O_4$ nRs with polyaniline provides a pathway to tailor the optical and electrical properties of the material. This enables new opportunities for applications that require specific optical absorption, emission, and electrical conductivity characteristics. Further research and development in this area can unlock the full potential of these doped nRs and expand their range of applications.

Because doping PANI with $ZnFe_2O_4$ nRs could lead to novel advancements in optoelectronics, photonics, and related fields, investigating the interactions and optical behavior of these materials is essential for understanding their potential and optimizing their performance. The molecular structure of PANI with $ZnFe_2O_4$ is represented in Scheme 1. Here, we doped PANI with 1, 3, and 5 wt. % of $ZnFe_2O_4$, and the structural, linear, and nonlinear optical properties have been determined. We believe our research outcomes will be useful in various applications such as optical sensors, optoelectronics, and photocatalysis.

2. Experimental Procedure

2.1. Material Preparation. Zinc nitrate ($Zn(NO_3)_2$), dimethylformamide (DFM), iron nitrate ($Fe(NO_3)_3$), aniline, and hydrochloric acid have been purchased from Sigma-Aldrich. The preparation of $ZnFe_2O_4$ nRs typically involves a synthesis process that starts with the reaction of appropriate precursor materials. $Zn(NO_3)_2$ and $Fe(NO_3)_3$ have been dissolved by using ethylene glycol, to form a mixed solution. Gradually heat at a temperature of 80°C for 8 hrs to enhance the crystallinity and structural properties of the nRs. Then, allow the solution to cool naturally. As it cools, the $ZnFe_2O_4$ nRs will precipitate out of the solution. These nRs can be collected by centrifugation and washed with DFM to remove any impurities. Finally, the collected $ZnFe_2O_4$ nRs are typically dried to remove any remaining solvent. For preparing PANI/($x = 1$, 3, and 5%) $ZnFe_2O_4$ nRs, PANI and $ZnFe_2O_4$ nRs have been dissolved in DMF. Sonicate the dispersion to ensure uniform mixing and suspension of the nRs. Dissolve the dopant material for PANI. Typically, chemical oxidants such as ammonium persulfate (APS) are used. Slowly add the dopant solution to the $ZnFe_2O_4$ nanoribbon dispersion while stirring continuously to ensure even mixing. The dopant initiates the polymerization of the PANI on the surface of the nRs, resulting in doping. Allow the doping reaction to proceed for a suitable amount of time, usually 6 hours, depending on the desired doping level and polymerization rate. Finally, dry the doped nRs under a vacuum or in a controlled environment to remove any remaining solvent.

2.2. Instrumentation. The X-ray diffraction pattern of our investigated composites was analyzed using a Philips X-ray diffractometer (model X'Pert). Monochromatic CuKα radiation was used at 40 kV and 25 mA. The chemical structures of the as-deposited and doped composites were investigated using Fourier-transform infrared spectroscopy (FTIR) in the 400–4000 cm^{-1} spectral range. The infrared spectrophotometer had a spectral resolution of $\pm 1\ cm^{-1}$ during the experiment. The optical spectroscopy of PANI@$ZnFe_2O_4$ nRs films (with varying percentages of PANI: $x = 1$, 3, and 5%) was conducted using a JASCO V-570 UV-Vis-NIR spectrophotometer. Thin films of PANI were fabricated by a thermal evaporation method using an Edwards E306A coating unit. The films were deposited onto optic flat quartz substrates that were previously cleaned. The

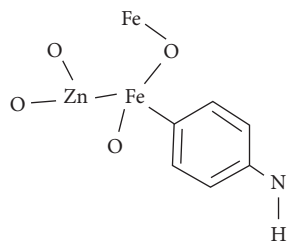

Scheme 1: Molecular structure of PANI doped by $ZnFe_2O_4$.

substrate was placed on a rotatable holder to ensure uniform fabrication at 25 cm from the evaporator. The deposition rate was controlled to be 5 nm/s, and the film thickness was 315 nm, monitored by a quartz crystal thickness monitor. The image of the deposited NS complex thin film on a glass substrate was examined using a scanning electron microscope (JSM-6360 LA, JEOL Ltd).

3. Results and Discussion

3.1. Structural Characterization

3.1.1. X-Ray Diffraction (XRD). The crystalline phase of materials, crystallinity degree, and grain sizes are the essential functions of the XRD [18]. The XRD of pure PANI and PANI @ x wt. % $ZnFe_2O_4$ ($x = 1$, 3, and 5) is illustrated in Figure 1(a). As we can see from Figure 1(a), the XRD spectra of pure PANI have two distinct sharp peaks at $2\theta^{\circ}$ equal to 19.4° and 26.3° with planes of (010) and (200) [19]. For PANI doped by $ZnFe_2O_4$ nR, there are peaks at $2\theta^{\circ}$ equal to 30°, 37°, 43°, 57°, and 65° with planes of (220), (311), (400), (440), and (551), respectively [20, 21]. The exited sharp peaks in the XRD pattern after the doping of $ZnFe_2O_4$ nRs assured the crystallinity of the composites which will affect the light propagation and decrease the scattering. Figure 1(b) shows the XRD spectra of $ZnFe_2O_4$; the peaks that appeared in the figure were completely consistent with the peaks that appeared in the samples after doping. The XRD technique detected two distinct peaks associated with PANI and additional peaks related to $ZnFe_2O_4$ after the doping process with a slight shift. The appearance of peaks related to $ZnFe_2O_4$ suggests that the doping process successfully introduced this material into the PANI structure. The presence of $ZnFe_2O_4$ peaks in various locations suggests that $ZnFe_2O_4$ is interacting with PANI. The XRD results indicate the successful doping of PANI with $ZnFe_2O_4$, resulting in the formation of a composite material with both PANI and $ZnFe_2O_4$ phases present.

The crystallinity degree of our investigated samples could be calculated by [22]

$$X_c\,(\%) = \frac{A_c}{A_c + A_a} \times 100, \tag{1}$$

where "A_c" and "A_a" refer to the total crystalline region and the total amorphous region, respectively. The average degree of crystallinity of PANI @x wt. % $ZnFe_2O_4$ ($x = 0$, 1, 3, and 5) is 56%, 67%, 69%, and 72%, respectively. By applying Scherrer's equation [23] to all the planes shown above, it is demonstrated that the average crystallite size of PANI @x wt. % $ZnFe_2O_4$ ($x = 0$, 1, 3, and 5) is 65, 74.5, 77, and 78 nm, respectively. The values of the total crystalline region and the total amorphous region are listed in Table 1. The crystal lattice exhibits minimal crystal defects, indicating a high level of crystallinity.

3.1.2. Thermal Gravimetric Analysis (TGA). TGA was used to calculate the weight loss of the nanocomposites at different temperatures. In Figure 2, the thermal analysis of pure PANI and PANI @ x wt. % $ZnFe_2O_4$ ($x = 1$, 3, and 5) is shown, revealing two main phases of mass degradation. Between 100°C and 280°C, there was a mass loss for pure PANI and PANI @ x wt. % $ZnFe_2O_4$ ($x = 1$, 3, and 5) equal to 50% and 28%, respectively. Between 280°C and 500°C, a mass loss for pure PANI and PANI @ x wt. % $ZnFe_2O_4$ ($x = 1$, 3, and 5) equal to 45% and 67%, respectively, was observed. There are two primary processes that could account for this degradation: first, the removal of water molecules adsorbed on the surface of PANI@ $ZnFe_2O_4$; second, the partial thermal degradation of organic volatile traces; and the complete decomposition of PANI@ $ZnFe_2O_4$, resulting in a residual mass. It is evident that PANI@ $ZnFe_2O_4$ exhibits exceptional thermal stability. We can conclude that the doping of PANI with $ZnFe_2O_4$ nRs can enhance the interfacial interactions between the two components. This improved interfacial adhesion can provide a more stable matrix structure and enhance the thermal stability of the composite. The strong bonding between PANI and $ZnFe_2O_4$ can prevent the release of volatile components and improve the thermal decomposition resistance.

3.1.3. SEM. Scanning electron microscope (SEM) is the most effective tool used by researchers for investigating the surface of the samples. The surface morphology of pure PANI and PANI@5 wt. % $ZnFe_2O_4$ is introduced in Figure 3. As we can see from the SEM images of pure PANI, the grains have a spherical shape. However, in the SEM image of PANI@5 wt. % $ZnFe_2O_4$, the grains exhibit an irregular cylindrical shape. The homogeneity of the grains in PANI@5 wt. % $ZnFe_2O_4$ showed the successful combination of PANI and $ZnFe_2O_4$.

3.1.4. FTIR. The Fourier-transform infrared spectroscopy (FTIR) spectrum is helpful in evaluating the vibrations of atoms, the structure of compounds, and the identification of functional groups. Figure 4 depicts the FTIR spectra in the wavenumber region 4000–400 cm^{-1} for pure PANI@x wt. % $ZnFe_2O_4$ ($x = 0$, 1, 3, and 5) and pure $ZnFe_2O_4$. According to the FTIR analysis of pure PANI, we can observe the following. Peaks between 3300 and 3500 cm^{-1} indicate the presence of amino (NH2) or imine (N=C) groups in PANI. Peaks between 3000 and 3100 cm^{-1} correspond to the stretching vibrations of carbon-hydrogen bonds, indicating the presence of aromatic rings in PANI [24]. Peaks appearing between 1600 and 1650 cm^{-1} suggest the presence of imine groups (N=C) in PANI. Peaks in the range of 1400–1600 cm^{-1} indicate the presence of aromatic carbon-

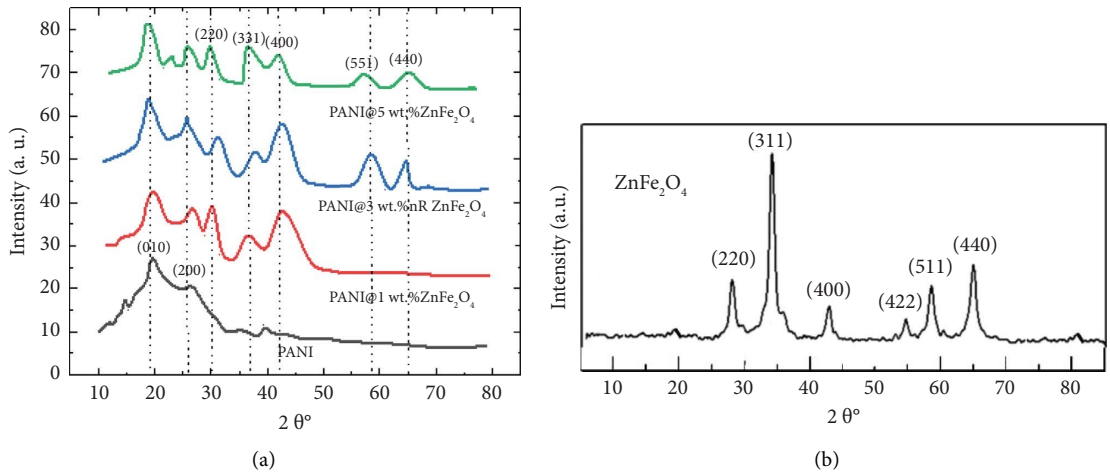

Figure 1: XRD pattern for (a) PANI@x wt. % $ZnFe_2O_4$ ($x = 0$, 1, 3, and 5) and (b) pure $ZnFe_2O_4$.

Table 1: Significant constants for PANI@x wt. % $ZnFe_2O_4$ ($x = 0$, 1, 3, and 5).

Sample PANI@ x wt.% $ZnFe_2O_4$	A_a	A_c	E_{g1} (eV)	E_{g2} (eV)	n_o	$X^{(3)}$ (10^{-12} esu)	n_2 (10^{-11} esu)
$X = 0$	433.9	553.5	0.49	1.98	2.54	5.93	8.81
$X = 1$	329.4	669.5	0.42	1.79	2.75	7.78	11.51
$X = 3$	307.2	685.4	0.42	1.77	3.07	18.12	17.93
$X = 5$	277.4	714.5	0.41	1.77	3.33	25.66	21.02

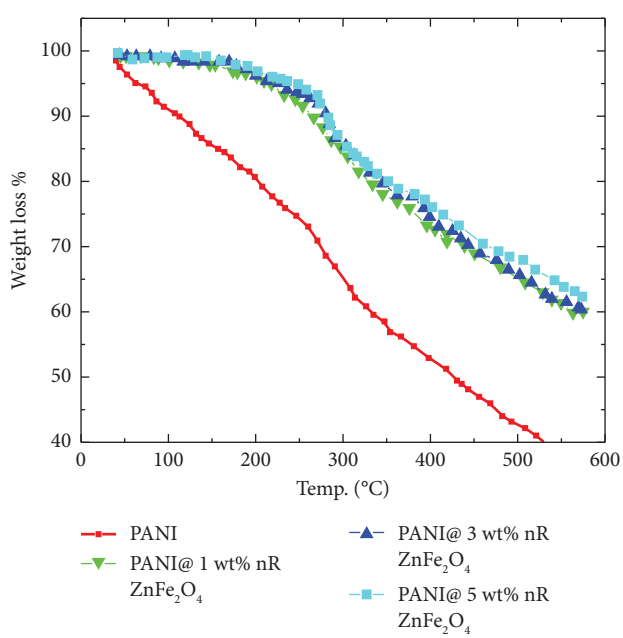

Figure 2: TGA of pure PANI and PANI@x wt. % $ZnFe_2O_4$ ($x = 1$, 3, and 5).

carbon (C-C) bonds in the polymer backbone. Peaks in the region of 700–900 cm^{-1} correspond to the bending vibrations of carbon-hydrogen bonds, providing further evidence of the presence of aromatic rings in PANI. The doping of $ZnFe_2O_4$ within PANI was introduced in peaks that generally appear at higher wavenumbers, often between 400 and 700 cm^{-1}, indicating the stretching vibrations of metal-oxygen bonds in the spinel structure.

Furthermore, the peaks around 580–700 cm^{-1} are typically associated with the stretching vibrations of iron-oxygen (Fe-O) bonds in $ZnFe_2O_4$ and the peaks in the range of 400–500 cm^{-1} suggest the presence of zinc-oxygen (Zn-O) bonds in the structure. As we can see from the FTIR of pure $ZnFe_2O_4$, three different significant absorption peaks 3440, 3100, and 1610 cm^{-1} correspond to O-H and C-H, C=O. The metal-oxygen (M-O) absorption peaks existed at 510 and 468 cm^{-1}. The PANI IR spectra that are typically analyzed focus on higher frequency ranges, from 800 cm^{-1} to 4000 cm^{-1}, where significant interactions occur. These ranges often include the characteristic peaks of N-H stretching, C-H stretching, C=C stretching, and C-N stretching which are significant in determining the different forms of polyaniline [25]. In the wavelength range between 400 and 700 cm^{-1}, it is usually associated with skeletal vibrations of the base structure, including bending, twisting, wagging, and rocking motions [26]. These vibrations can be quite complex and involve the movement of several atoms or groups of atoms within the molecule.

3.2. Linear Optical Properties. The process of absorbing UV light by organic materials provides valuable information regarding electron transitions between different energy levels. Therefore, a UV-Vis-NIR spectrophotometer is employed to investigate the optical characteristics of organic substances, such as PANI. Figure 5 shows the optical transmittance variation, T, with the wavelength for pure

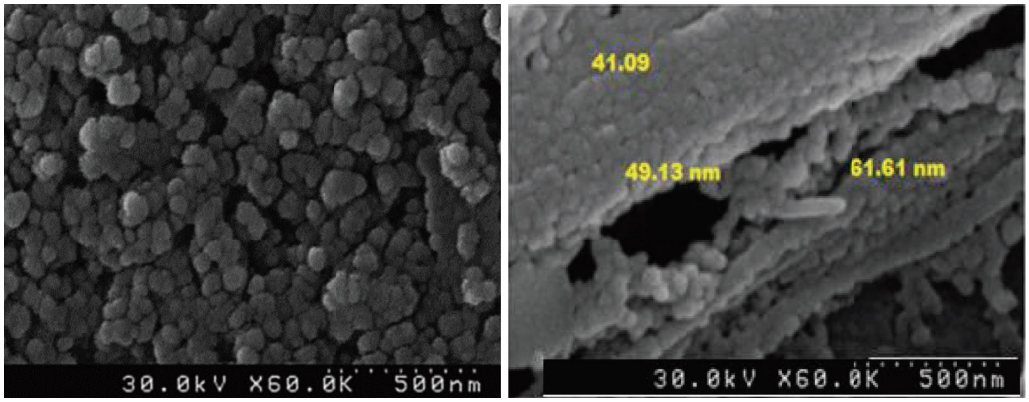

Figure 3: SEM for pure PANI and PANI@5 wt. % $ZnFe_2O_4$.

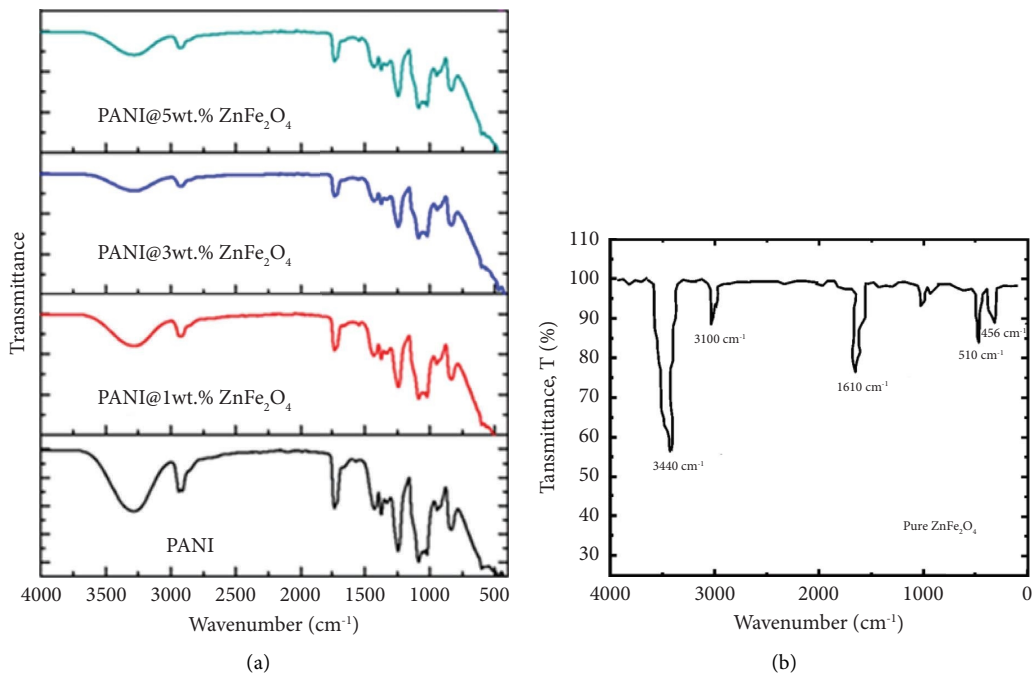

Figure 4: FTIR pattern for (a) pure PANI@x wt. % $ZnFe_2O_4$ ($x = 0$, 1, 3, and 5) and (b) pure $ZnFe_2O_4$.

PANI and PANI@x wt. % $ZnFe_2O_4$ ($x = 1$, 3, and 5). Figure 6 shows the optical reflectance, R, for our investigated samples. Based on the information presented in Figures 5 and 6, it can be inferred that T increased, while the R decreased when the $ZnFe_2O_4$ nR within PANI was increased. The enhancement in the light transmission could be a result of reduced light scattering or improved transparency of the composite material. The $ZnFe_2O_4$ nR might facilitate the formation of more uniform and stable PANI structures, leading to a decrease in light reflection. Furthermore, the specific interaction between PANI and $ZnFe_2O_4$ nR on a molecular level could also play a role. It is possible that the inclusion of nRs modifies the electronic structure or band gap of PANI, influencing its optical properties.

The extinction index, k, could be calculated using [27]

$$k = \frac{\alpha\lambda}{4\pi}, \tag{2}$$

where α is the light absorption and λ is the light wavelength. Figure 7 illustrates the extinction index, k, of pure PANI and PANI@x wt. % $ZnFe_2O_4$ ($x = 1$, 3, and 5). The increase in K of PANI doped with $ZnFe_2O_4$ nRs could be attributed to the introduction of an additional electronic state in the material, which can enhance its optical properties. This can lead to an increased absorption of light, resulting in a higher extinction index. Moreover, $ZnFe_2O_4$ nRs may possess unique optical properties themselves, such as a high dielectric constant or strong light scattering properties. When incorporated into PANI, these properties could further affect the overall extinction index of the composite material.

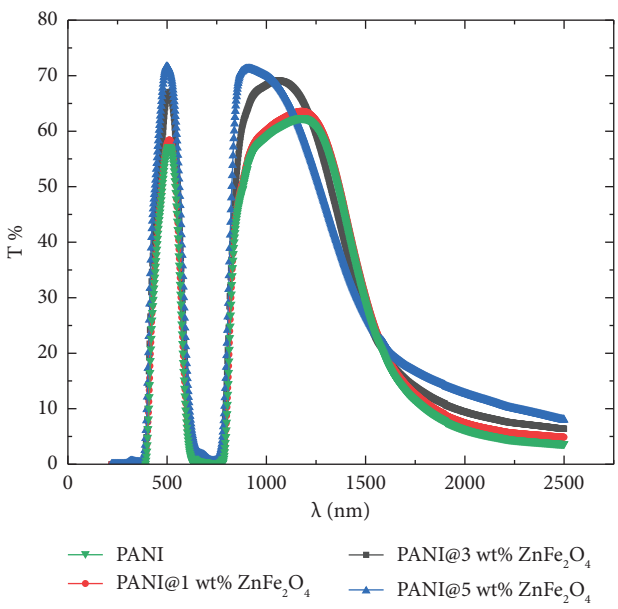

Figure 5: The optical transmittance of pure PANI and PANI@x wt. % $ZnFe_2O_4$ ($x = 1$, 3, and 5) versus wavelength.

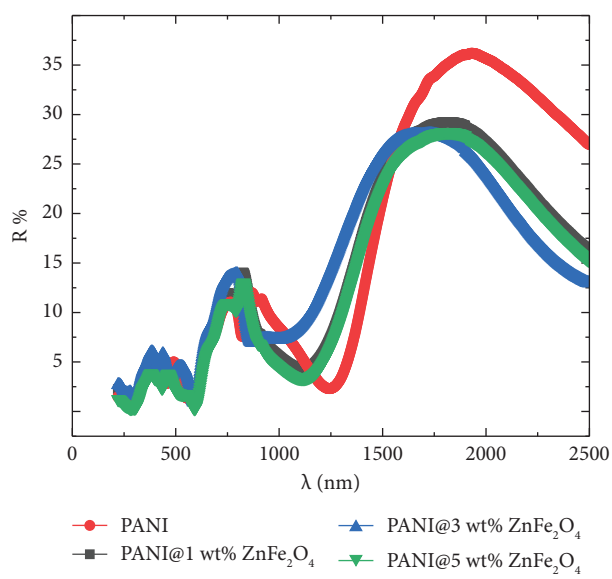

Figure 6: The optical reflectance of pure PANI and PANI@x wt. % $ZnFe_2O_4$ ($x = 1$, 3, and 5) variation with wavelength.

The refractive index, n, of our composites could be determined from [27]

$$n = \frac{(1+R) + \sqrt{4R - (1-R)^2 k}}{(1-R)}. \quad (3)$$

The refractive index variation of pure PANI and PANI@x wt. % $ZnFe_2O_4$ ($x = 1$, 3, and 5) with wavelength is depicted in Figure 8. The refractive index of PANI increases with the increase in doping of $ZnFe_2O_4$ nR. This could be related to $ZnFe_2O_4$ having a higher refractive index compared to PANI. When PANI incorporates $ZnFe_2O_4$ nanoparticles as

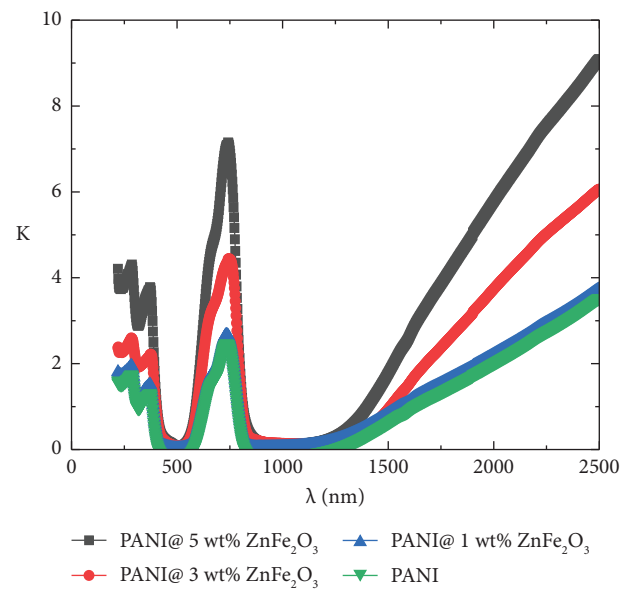

Figure 7: The extinction index of pure PANI and PANI@x wt. % $ZnFe_2O_4$ ($x = 1$, 3, and 5) variation with wavelength.

doping agents, the overall refractive index of the composite material increases due to the higher refractive index of $ZnFe_2O_4$. Nanoparticles are incorporated into the PANI matrix, resulting in a higher concentration of $ZnFe_2O_4$. As a result, the composite material's overall refractive index increases due to the increased concentration of the higher-index $ZnFe_2O_4$ component.

The absorption coefficient, α, could be calculated as [22]

$$\alpha = \frac{1}{x} ln\left(\frac{1-R}{T}\right), \quad (4)$$

where x is the film thickness. Figure 9 shows the absorption coefficient, α, for pure PANI and PANI@x wt. % $ZnFe_2O_4$ ($x = 1$, 3, and 5). The absorption coefficient of PANI increased with the increase in doping of ZnFe2O4, and this can be attributed to the strong light-absorbing properties of $ZnFe_2O_4$, especially in the visible and near-infrared regions. According to the Wemple-DiDomenico model, WDD, we can calculate the optical energy gap, Eg, of PANI and PANI@x wt. % $ZnFe_2O_4$ ($x = 1$, 3, and 5) by using [27, 28]

$$(\alpha h\nu)^{0.5} = A\left(h\nu - E_g^{opt}\right), \quad (5)$$

where A is a constant and the abscissa extrapolation will yield to the forbidden energy gap (E_g). According to (5), Figure 10 shows the relation between $(\alpha h\nu)^{0.5}$ and $h\nu$ for PANI and PANI@x wt.% $ZnFe_2O_4$ ($x = 1$,3, and 5). The figure indicates two strong absorptions in the range of 0.5 eV to 2.1 eV. At the small photon energy, the energy gap, Eg_1, is 0.5 eV. At the lower wavelength, the energy is 2.1 eV and the energy gap decreases with the increase of $ZnFe_2O_4$ doping. The decrease in the energy gap when doped with $ZnFe_2O_4$ could be attributed to the introduction of impurities into the crystal lattice. Doping is the process of intentionally adding impurity atoms to a semiconductor material to modify its

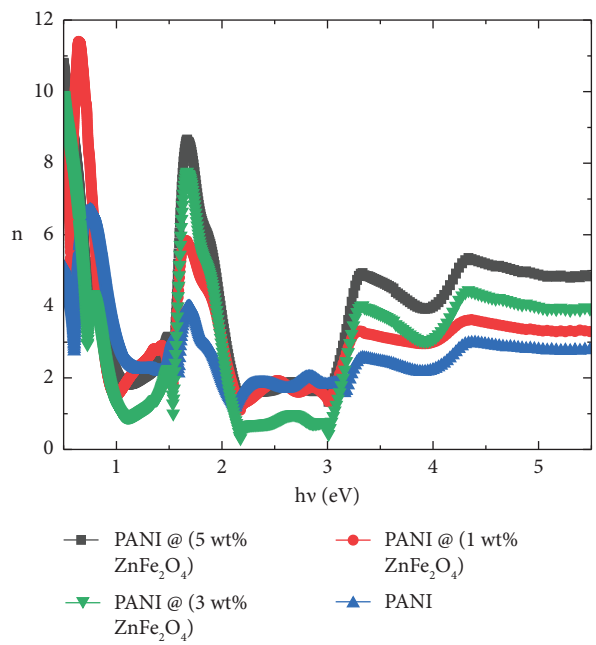

Figure 8: The refractive index of pure PANI and PANI@x wt. % $ZnFe_2O_4$ ($x = 1$, 3, and 5) variation with wavelength.

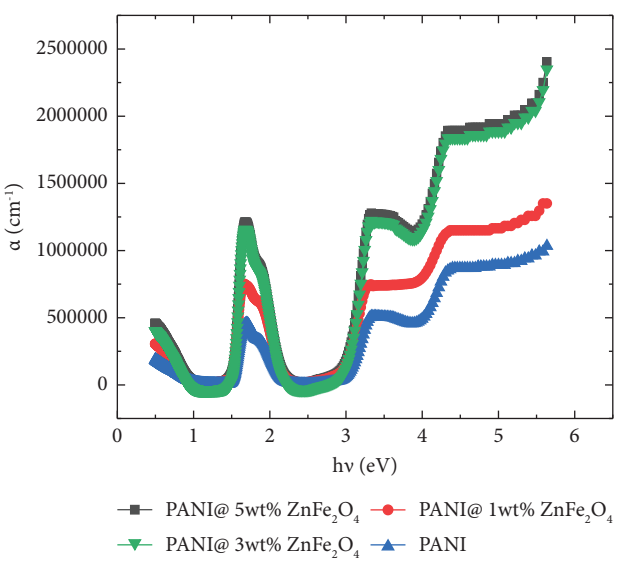

Figure 9: The absorption coefficient of pure PANI and PANI@x wt. % $ZnFe_2O_4$ ($x = 1$, 3, and 5) variation with wavelength.

optical and electrical properties. In this case, when $ZnFe_2O_4$ is doped, the impurity atoms of Zn and Fe replace some of the original atoms in the crystal lattice. The introduction of impurities can create energy levels within the band gap of the material, effectively reducing the energy gap between the valence band and the conduction band.

3.3. Dielectric Properties. The dielectric constants are related to the optical and electrical properties of the materials [29]. The dielectric constant, ε_1, relates the dielectric constant of a material to its refractive index and extinction coefficient, providing insight into its ability to store electric energy and absorb or dissipate energy as heat. The dielectric loss, ε_2, relates the dielectric loss of a material to the product of its refractive index and extinction coefficient, representing the energy dissipation or heat generation as light passes through the material. The dielectric constant, ε_1, and dielectric loss, ε_2, of PANI doped with $ZnFe_2O_4$ can be, respectively, calculated as follows [30]:

$$\begin{aligned} \varepsilon_1 &= n^2 - \kappa^2, \\ \varepsilon_2 &= 2n\kappa. \end{aligned} \tag{6}$$

Figure 11 shows the dielectric constant, ε_1 and ε_2, variation with the photon energy for pure PANI and PANI@x wt. % $ZnFe_2O_4$ ($x = 1$, 3, and 5). As noted from the figure, the values of ε_1 of our prepared samples are higher than those of ε_2, and this could be attributed to the rapid increase that has been measured in the refractive index values. The decrease in ε_1 and ε_2 at lower photon energy is associated with the dielectric decay within our synthesized materials. Additionally, ε_1 and ε_2 exhibit a dependence on $ZnFe_2O_4$ doping ratio, as they increase with increasing $ZnFe_2O_4$ doping ratio.

The volume energy loss function (VELF) and surface energy loss function (SELF) are quantities that are derived from the dielectric constant. They are used to analyze the energy losses that occur in a material when it is exposed to an electric field. They provide insights into the dissipation of energy as heat within the material. VELF and SELF are calculated using [23]

$$\begin{aligned} \text{VELF} &= \frac{\varepsilon_2}{\varepsilon_1^2 - \varepsilon_2^2}, \\ \text{SELF} &= \frac{\varepsilon_2^2}{(\varepsilon_1 + 1)^2 + \varepsilon_2^2}. \end{aligned} \tag{7}$$

Volume energy loss function and surface energy loss function with the photon energy for pure PANI and PANI@ x wt. % $ZnFe_2O_4$ ($x = 1$, 3, and 5) are shown in Figure 12. The data indicated that the free charge carriers lose energy in a similar manner to when they move across the surface, particularly at lower energy levels.

3.4. Nonlinear Optical Properties. The nonlinear optical behavior occurs due to the interaction between the atomic oscillators of materials and high-intensity light. Organic materials with strong nonlinear properties find various applications in industries such as communications and data storage [31]. The third-order nonlinear optical susceptibility, $\chi^{(3)}$, and the nonlinear refractive index, n_2, are calculated using Miller's principle [32, 33]:

$$\begin{aligned} \chi^{(3)} &= \frac{A(n^2 - 1)^4}{4\pi^4}, \\ n_2 &= \frac{12\pi}{n_o}\chi^3. \end{aligned} \tag{8}$$

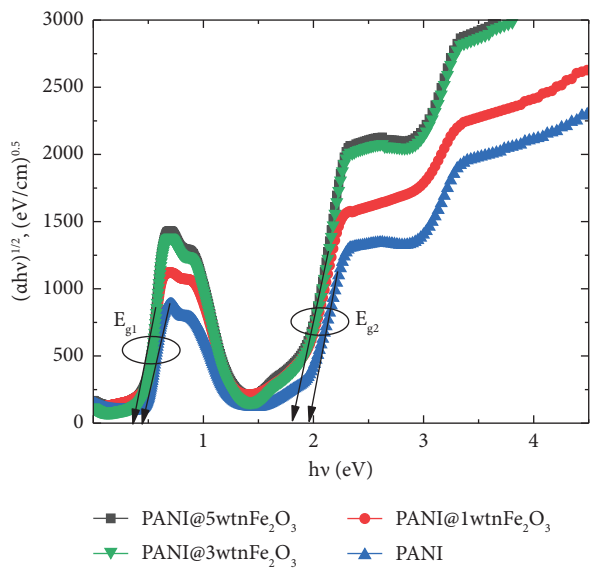

Figure 10: $(\alpha h\nu)^{0.5}$ variation with the photon energy for pure PANI and PANI@x wt. % $ZnFe_2O_4$ ($x = 1$, 3, and 5) variation with wavelength.

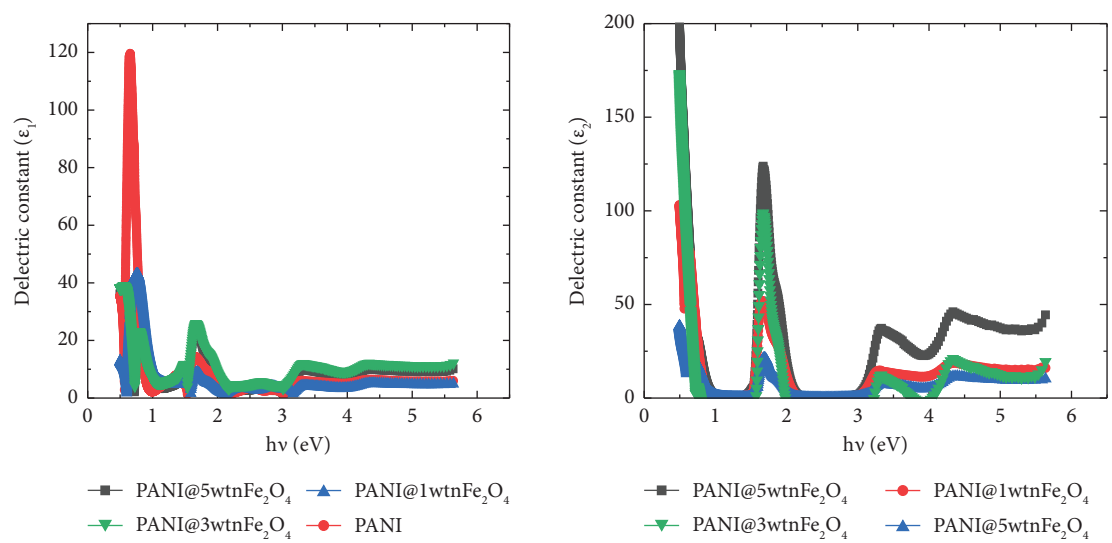

Figure 11: Dielectric constant variation with the photon energy for pure PANI and PANI@x wt. % $ZnFe_2O_4$ ($x = 1$, 3, and 5).

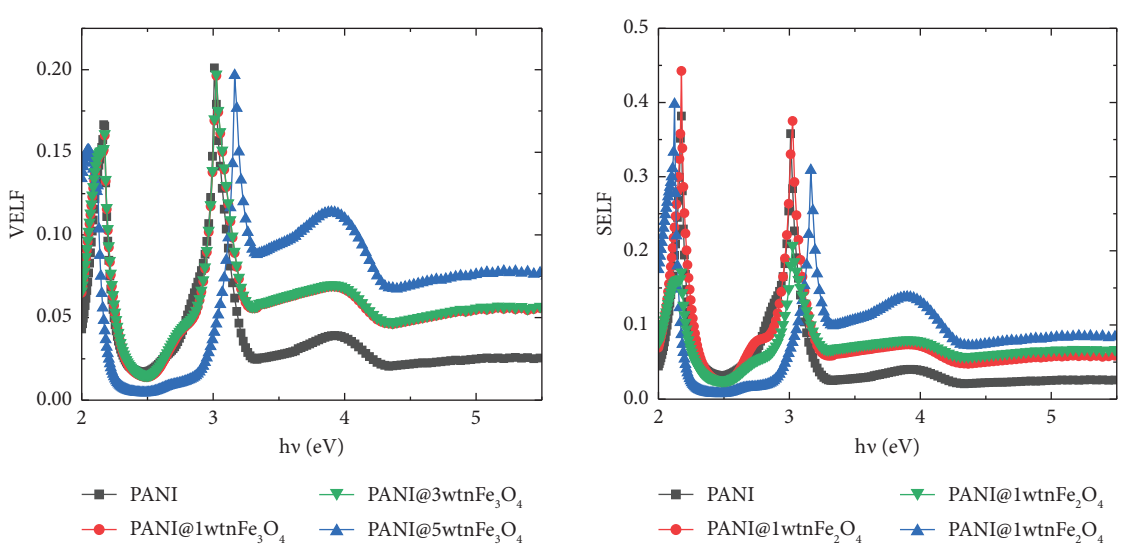

Figure 12: Volume and surface energy loss function with the photon energy for pure PANI and PANI@x wt. % $ZnFe_2O_4$ ($x = 1$, 3, and 5).

Table 1 shows the values of $\chi^{(3)}$ and n_2 for pure PANI and PANI@x wt. % $ZnFe_2O_4$ ($x = 1$, 3, and 5). As noted from the table, the values of $\chi^{(3)}$ and n_2 showed similar behavior, and their values increased with the increase in $ZnFe_2O_4$ within PANI. Doping PANI with $ZnFe_2O_4$ introduces new charge carriers and alters the electronic and optical properties of the composite material. $ZnFe_2O_4$ nanoparticles can act as electron acceptors, leading to charge transfer and modification of the electronic structure of PANI. This charge transfer can enhance the nonlinear optical effects and increase the susceptibility of the composite material. Moreover, $ZnFe_2O_4$ nanoparticles have unique properties that contribute to the enhanced nonlinear optical response. For example, $ZnFe_2O_4$ nanoparticles possess a wide band gap and high refractive index and exhibit superparamagnetic behavior. These characteristics can lead to stronger nonlinear optical phenomena, such as higher third-order susceptibility and enhanced nonlinear refractive index.

4. Conclusion

To improve the structural, linear, and nonlinear optical properties of PANI, a thin film of PANI@x wt. % $ZnFe_2O_4$ ($x = 1$, 3, and 5) has been fabricated. XRD, SEM, TGA, and FTIR have been utilized to investigate the structural properties of our thin film samples. The XRD results showed an increase in the degree of crystallinity for PANI @5 wt. % $ZnFe_2O_4$ by about 16%. The UV spectrophotometer has been used to study the optical transmission and reflection for PANI@x wt. % $ZnFe_2O_4$ ($x = 1$, 3, and 5). The results showed that $ZnFe_2O_4$ nRs might facilitate the formation of more uniform and stable PANI structures, leading to a decrease in light reflection. The nonlinear optical results assured that the values of $\chi^{(3)}$ and n_2 increased with the increase in $ZnFe_2O_4$ within PANI. Doping PANI with $ZnFe_2O_4$ introduces new charge carriers and alters the electronic and optical properties of the composite material. The results of our thesis suggest that a mixture of 5 weight percent of $ZnFe_2O_4$ and PANI can be used in various applications, such as optical, electrochemical, optoelectronics, and photocatalysis.

Data Availability

The datasets generated and analyzed during the current study are available from the corresponding author upon reasonable request.

Conflicts of Interest

The authors declare that there are no conflicts of interest.

Acknowledgments

The authors would like to acknowledge the University of Tabuk for the financial support under research project no. S-270-1440.

References

[1] Z. He, H. Xie, H. Wu et al., "Recent advances in MXene/polyaniline-based composites for electrochemical devices and electromagnetic interference shielding applications," *ACS Omega*, vol. 6, no. 35, pp. 22468–22477, 2021.

[2] S. I. Abd Razak, I. F. Wahab, F. Fadil et al., "A review of electrospun conductive polyaniline based nanofiber composites and blends: processing features, applications, and future directions," *Advances in Materials Science and Engineering*, vol. 2015, Article ID 356286, 19 pages, 2015.

[3] G. Liao, Q. Li, and Z. Xu, "The chemical modification of polyaniline with enhanced properties: a review," *Progress in Organic Coatings*, vol. 126, pp. 35–43, 2019.

[4] S. Li, M. Meng Lin, M. S. Toprak, D. K. Kim, and M. Muhammed, "Nanocomposites of polymer and inorganic nanoparticles for optical and magnetic applications," *Nano Reviews*, vol. 1, no. 1, p. 5214, 2010.

[5] B. S. Khened, M. V. N. Prasad, and M. Sasikala, "Synthesis, characterization and liquid petroleum gas sensing of $ZnFe_2O_4$ nanoribbons doped polyaniline nanocomposites," *Sensor Letters*, vol. 14, no. 8, pp. 817–823, 2016.

[6] N. Tyagi, A. Kumar, S. Chaudhry, S. Ray, and G. Varma, "Synthesis of 1-D Nanostructures of ZnFe₂O₄ and ZnO by a Low Cost Self-Catalyzed CVD Method," *Advanced Materials Research*, vol. 67, pp. 265–270, 2009.

[7] Y. Xiang, Y. Huang, B. Xiao, X. Wu, and G. Zhang, "Magnetic yolk-shell structure of ZnFe2O4 nanoparticles for enhanced visible light photo-Fenton degradation towards antibiotics and mechanism study," *Applied Surface Science*, vol. 513, Article ID 145820, 2020.

[8] Y. Duan, H. Pang, and H. Zhang, "Structure and composition design on ternary CNT@ ZnFe2O4@ ZnO composite utilized as enhanced microwave absorbing materials," *Diamond and Related Materials*, vol. 120, Article ID 108701, 2021.

[9] G. Yuan, K. Li, J. Zhang et al., "A novel insight into the microwave induced catalytic reduction mechanism in aqueous Cr (VI) removal over ZnFe2O4 catalyst," *Journal of Hazardous Materials*, vol. 443, Article ID 130211, 2023.

[10] M. Yagmurcukardes, F. M. Peeters, R. T. Senger, and H. Sahin, "NRs: from fundamentals to state-of-the-art applications," *Applied Physics Reviews*, vol. 3, p. 4, 2016.

[11] S. Kumar, S. Pratap, V. Kumar, R. K. Mishra, J. S. Gwag, and B. Chakraborty, "Electronic, transport, magnetic, and optical properties of graphene nanoribbons and their optical sensing applications: a comprehensive review," *Luminescence*, vol. 38, no. 7, pp. 909–953, 2022.

[12] S.-Y. Tong, J.-M. Wu, M.-J. Tung, W.-S. Ko, Y. T. Huang, and Y.-P. Wang, "Effect of Ni concentration on electromagnetic wave absorption of (Ni, Mn, Zn) Fe2O4/resin particulate composites," *Journal of Alloys and Compounds*, vol. 525, pp. 143–148, 2012.

[13] A. H. Alshammari and T. A. Taha, "Structure, thermal and dielectric insights of PVC/PVP/ZnFe2O4 polymer nanocomposites," *The European Physical Journal Plus*, vol. 136, no. 12, p. 1201, 2021.

[14] X. Li, "Enhanced electromagnetic wave absorption properties of ZnFe2O4 nanoribbon/polyaniline composites," *Journal of Alloys and Compounds*, vol. 821, p. 153446, 2020.

[15] E. F. M. El-Zaidia, H. A. M. Ali, T. A. Hamdalla, A. A. A. Darwish, and T. A. Hanafy, "Optical linearity and bandgap analysis of Erythrosine B doped in polyvinyl alcohol films," *Optical Materials*, vol. 100, Article ID 109661, 2020.

[16] A. A. A. Darwish, S. I. Qashou, A. G. K. Alenezy et al., "Preparation and characterizations of Erbium (III)-Tris (8-hydroxyquinolinato) nanostructured films for possible use in gas sensor," *Sensors and Actuators A: Physical*, vol. 340, Article ID 113550, 2022.

[17] X. Zhu, J. Zhang, J. Liu, and Y. Zhang, "Recent progress of rare-earth doped upconversion nanoparticles: synthesis, optimization, and applications," *Advanced Science*, vol. 6, Article ID 1901358, 22 pages, 2019.

[18] S. A. Al-Ghamdi, T. A. Hamdalla, E. El-Zaidia et al., "Structural, electronic, and optoelectronic characteristics of GaClPc/n-Si heterojunction for photodiode device," *Materials Science in Semiconductor Processing*, vol. 147, Article ID 106704, 2022.

[19] A. Mostafaei and A. Zolriasatein, "Synthesis and characterization of conducting polyaniline nanocomposites containing ZnO nanorods," *Progress in Natural Science: Materials International*, vol. 22, no. 4, pp. 273–280, 2012.

[20] A. R. Abbasian and M. S. Afarani, "One-step solution combustion synthesis and characterization of ZnFe 2 O 4 and ZnFe 1.6 O 4 nanoparticles," *Applied Physics A*, vol. 125, pp. 1–12, 2019.

[21] R. C. Sripriya, A. Ezhil, J. Madhavan, and A. Raj Victor, "Synthesis and Characterization studies of ZnFe2O4 nanoparticles," *Mechanics, Materials Science & Engineering Journal*, vol. 9, p. 1, 2017.

[22] A. M. Alsharari, S. I. Qashou, R. A. S. Alobaidi et al., "Effectiveness of annealing on the structural, electrical, and optical properties of erbium (III)-tris (8-hydroxyquinolinato) films for possible use in OLEDs," *Journal of Inorganic and Organometallic Polymers and Materials*, vol. 32, no. 8, pp. 3235–3243, 2022.

[23] A. A. A. Darwish, T. A. Hamdalla, E. F. M. El-Zaidia, T. A. Hanafy, S. A. Issa, and I. S. Yahia, "Thin films of nanostructured gallium (III) chloride phthalocyanine deposited on FTO: structural characterization, optical properties, and laser optical limiting," *Physica B: Condensed Matter*, vol. 593, Article ID 412321, 2020.

[24] E. A. Ponzio, R. Echevarria, G. M. Morales, and C. Barbero, "Removal of N-methylpyrrolidone hydrogen-bonded to polyaniline free-standing films by protonation–deprotonation cycles or thermal heating," *Polymer International*, vol. 50, no. 11, pp. 1180–1185, 2001.

[25] Singu, S. Bal, P. Srinivasan, and P. Srinivas, "Benzoyl peroxide oxidation route to nano form polyaniline salt containing dual dopants for pseudocapacitor," *Journal of the Electrochemical Society*, vol. 159, no. 1, p. A6, 2011.

[26] V. A. Bershtein and V. A. Ryzhov, "Far infrared spectroscopy of polymers," *Polymer Analysis and Characterization*, Springer, Berlin, Heidelberg, 2005.

[27] A. M. Hassanien, A. A. A. Darwish, A. M. Kamal, M. Al-Gawati, and T. A. Hamdalla, "Annealing effect on the morphology, linear and non-linear optical properties of squaraine derivative thin films for optoelectronics applications," *Optical Materials*, vol. 142, Article ID 114033, 2023.

[28] S. P. Ashokkumar, H. Vijeth, L. Yesappa, M. Niranjana, M. Vandana, and H. Devendrappa, "Electrochemically synthesized polyaniline/copper oxide nano composites: to study optical band gap and electrochemical performance for energy storage devices," *Inorganic Chemistry Communications*, vol. 115, Article ID 107865, 2020.

[29] M. Caglar, S. Ilican, Y. Caglar, and F. Yakuphanoglu, "Electrical conductivity and optical properties of ZnO nanostructured thin film," *Applied Surface Science*, vol. 255, no. 8, pp. 4491–4496, 2009.

[30] S. A. Al-Ghamdi, A. A. A. Darwish, T. A. Hamdalla et al., "Preparation of TlInSe2 thin films using substrate temperature: characterization, optical and electrical properties," *Optical Materials*, vol. 129, Article ID 112514, 2022.

[31] D. J. Williams, "Organic polymeric and non-polymeric materials with large optical nonlinearities," *Angewandte Chemie International Edition in English*, vol. 23, no. 9, pp. 690–703, 1984.

[32] A. A. A. Darwish, S. I. Qashou, E. F. M. El-Zaidia et al., "Electrical and photoelectrical properties of a vacuum-deposited MnClPc/n-Si heterojunction for photodiode application," *Micro and Nanostructures*, vol. 167, Article ID 207239, 2022.

[33] M. Benhaliliba, A. Ben Ahmed, M. Kaleli, and S. E. Meftah, "Structural, optical, nonlinear optical, HUMO-LUMO properties and electrical characterization of Poly (3-hexylthiophene)(P3HT)," *Optical Materials*, vol. 132, Article ID 112782, 2022.